Structural and optical properties of $ZnTe$ thin films induced by plasma immersion O^- ion implantation

A. M. Aboraia[1], **M. Ahmad**[1], **E. A. Abdel Wahab**[1], **H. Shokry Hassan**[2] **and E. R. Shaaban**[1,*]

[1]Department of Physics, Faculty of Science, Al-Azahar University, 71542 Assiut, Egypt.
[2]Advanced Technology and New Materials Research Institute, City of Scientific Research and Technology Applications, New Borg El-Arab City, Alexandria 21934, Egypt.

Abstract: Various thickness of Zinc telluride ($ZnTe$) thin films were deposited onto glass substrates in terms of the thermal evaporation technique. The experiments XRD of both powder and thin films of $ZnTe$ showed that the films are polycrystalline and have a zinc blende (cubic) structure. The effect of exposure to the oxygen plasma-immersion-ion-implantation ($O^- - PIII$) on the structural and optical constants of the same samples of different thicknesses were also investigated. It is observed that the oxygen $PIII$ treatment can reduce both crystallize size and microstrain of $ZnTe$ thin films. It is also observed that the oxygen $PIII$ treatment can effectively improve the transmission spectra of the samples particularly in medium and transparent regions, therefore the refractive index decrease. The optical constants and energy gap of different thickness of $ZnTe$ have been determined before and after oxygen plasma-immersion-ion-implantation ($O^- - PIII$). It is observed that the oxygen $PIII$ treatment can effectively improve the transmission spectra of the samples particularly in medium and transparent regions, therefore the refractive index decrease. In addition, the optical band gap has been determined before and after $O^- - PIII$. The $O^- - PIII$ causes an increase in the energy gap of different thickness of $ZnTe$ thin films.

Keywords: Zinc telluride; Thin film; $O^- - PIII$; Optical constants; Optical band gap; Plasma application.

1 Introduction

Chalcogenide glass is a glass containing one or more *chalcogenide* elements (not counting oxygen). The name *chalcogenide* originates from the Greek word "*chalcos*" meaning ore and "gen" meaning formation, thus the term chalcogenide is generally considered to mean ore former [1]. These are three elements in Group 16 in the periodic table: sulfur, selenium and tellurium.

Zinc Telluride ($ZnTe$) is a compound of chalcogenide, which is interesting in optoelectronic materials [2,3]. Zinc telluride is an important semiconducting material for the development of various modern solid state devices (blue light emitting diodes, laser diodes, solar cells, microwave devices, etc.) [4,5]. It is a direct band gap semiconductor having band gap $2.26eV$ at $300K$ and usually a p-type semiconductor. It has potential applications in electronic and optical devices [6]. Moreover, the optical properties are closely related to the structure of the films and study of the optical properties gives valuable information about the $ZnTe$ properties.

Plasma Immersion Ion Implantation ($PIII$) process is a three dimensional surface modification method that is quite mature and well known to the surface engineering community nowadays, specially to those working in the field of plasma-materials interaction, aiming at both industrial and academic applications.

Plasma Immersion Ion Implantation and deposition ($PIII\&D$) is becoming a routine method of surface modification, with the advantage of pushing up the retained dose levels limited by the sputtering owing to ion implantation. Therefore, well adherent, thick, three-dimensional films without stress are possible to be achieved, at relatively low cost, using $PIII\&D$. The gas plasma treatments have been probed as a suitable technology for the modification on the optical characteristic of the films [7,8,9].

The present work has a fourfold targets; the first was the effect of film thickness in microstructure parameters (crystallites size and microstrain) of $ZnTe$ thin films, the second was the effect of film thickness in optical

---

* Corresponding author e-mail: esam_ramadan2008@yahoo.com

constants of *ZnTe* thin films, the third was examine the changes in in microstructure parameters and the optical constants of *ZnTe* thin films after the oxygen plasma-immersion-ion-implantation $(O^- - PIII)$ and the fourth was an interpretation of optical constant before and after $(O^- - PIII)$ in terms of the microstructure parameters of the *ZnTe* thin films. Film thickness and refractive index have been obtained in terms of Swanepoel's method [8], which is based on the use of the extremes of the interference fringes of *ZnTe* thin films before and after $(O^- - PIII)$. The energy gap has been determined in terms of Transmission and reflection spectrum in strong absorption region.

2 Experimental

Zinc Telluride (*ZnTe*) powder of Aldrich Chemical Co. make having purity of $> 99.999\%$ was used. The glass thin films were deposited by evaporating Zinc Telluride (*ZnTe*) from a resistance heating quartz glass crucible onto clean glass substrates kept at room temperature, using a conventional coating unit (Denton Vacuum DV $502A$) and a vacuum of about $2x10^{-6}$ Torr. The evaporation rate as well as the film thickness was controlled using a quartz crystal $DTM100$ monitor. The mechanical rotation of the substrate holder $(\approx 30 rpm)$ during deposition produced homogeneous film. The temperature rise of the substrate owing to radiant heating from crucible was negligible. Small fluctuations in the measured transmittance $(\approx 1.0\%)$ of studied films confirm their homogeneity. The mechanical rotation of the substrate holder was about $\approx 30 rpm$ during deposition produced in order to raise the homogeneity of film. Both the deposition rate and the film thickness were controlled using a quartz crystal monitor $DTM100$. The deposition rate was maintained $20A^o/s$ during the sample preparations.

The structure of the prepared powder and thin films were examined by XRD analysis (Philips X-ray diffractometry (1710)) with Nifiltered Cu Ka radiation with $(\lambda = 0.15418 nm)$.The intensity data were collected using the step scanning mode with a small interval $(\Delta 2\theta = 0.02^o)$ with a period of $5s$ at each fixed value to yield reasonable number of counts at each peak maximum. The transmittance and reflectance measurements were carried out using a double-beam $(JascoV670)$ spectrophotometer, at normal incidence of light and in a wavelength range between 300 and $2500 nm$. Without a glass substrate in the reference beam, the measured transmittance spectra were used in order to calculate the refractive index and the film thickness of *ZnTe* thin films according to Swanepoel's method.

The experimental setup of the present plasma is consists of three main parts, discharge cell, electrical discharge circuit and the high vacuum system as shown in Fig. (1). The discharge cell consists of two movable parallel electrodes enclosed in a vacuum vessel. Each
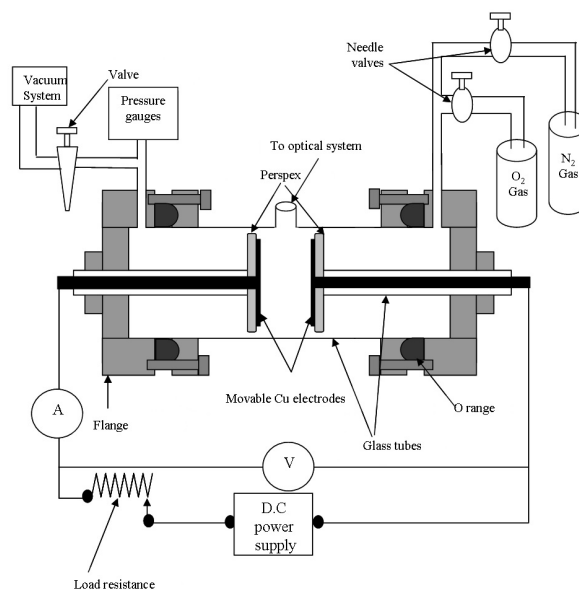

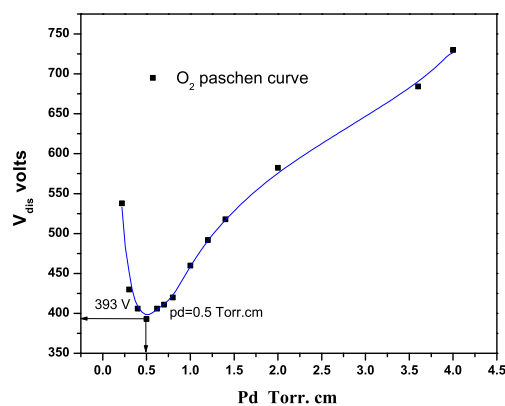**Fig. 1:** Schematic diagram of electric discharge cell.

Fig. 2: The well-known Paschen curve for oxygen gas.

electrode consists of a disk of copper of $5cm$ diameter coating with Perspex to prevent the discharge from the back of the electrode. The vessel consists of cylindrical Perspex tube with outside diameter $11cm$ and length $12cm$. It has two open holes one is connected to the vacuum system and other to the used gases. The electrical discharge circuit consists of, a DC power supply (high voltage power supply), which operate in range $(0 - 2000 volt, 200 mA)$. The discharge current in the circuit was measured by digital multimeter $(SK - 6160)$, the voltage on the discharge tube was measured by digital multimeter $(KIT - 2704B)$. The high vacuum system consists of two stages Edward rotary pump, diffusion pump and vacuum gauges. The vacuum gauge of type

pirani-pinning 1005, which consists of two heads of pirani ($PRM10K$) standard pressure gauge head range $760 to 10 - 3 torr$ and one pinning model ($CO25K$) of range 10^{-3} to $10^{-7} torr$. Fig. (2) shows the well-known Paschen curve for oxygen gas. The curve have a minimum point at $pd = 0.5 torr.cm$ and the discharge voltage VBr = 393 volts. At low pressure the collision frequency is low, so that sufficient ionization is maintained only by increasing the probability of ionization at each collision; consequently the electron velocity, and the electric field must be high, hence VBr must increase as p decreases. At the higher pressure the collision frequency is high and the rate of energy loss correspondingly high. Thus VBr must be increased to overcome the loss of energy for given distance d, and the curve must have a minimum value [10]. The thin film sample was put between the two electrodes in the NG (Negative Glow) region. The vessel evacuated to $10^{-3} torr$ after that the O_2 gas inlet to the vessel, the operating pressure were kept at $p = 0.5 torr$. The discharge current kept at $100 mA$ during the experiment which generates discharge power of $45 watt$. The thin film immerses two minutes in the plasma.

3 Results and discussion

3.1 X-ray analysis and microstructure parameters of ZnTe before and after $O^- PIII$

Both the X-ray diffractogram of $ZnTe$ powder and simulated $ZnTe$ cards according to ($JCPDS$ Data file: $01 - 0582 - cubic$) are shown in Fig. (3), which exhibit a polycrystalline nature. Fig. (2) illustrates the XRD patterns of $ZnTe$ thin films of different thicknesses on glass substrates before $O^- - PIII$. This figure shows that the X-ray diffraction (XRD) analysis of $ZnTe$, that revealed that the films are polycrystalline of zinc-blende structure with peaks at $\Delta 2\theta = 25.42^o, 42.20^o and 49.87^o$ corresponding to $C(111), C(220) and C(311)$ orientations, respectively ($JCPDS$ Data file: $01 - 0582 - cubic$).

Fig. (4) also displays that the intensity of the peak increases with increasing film thickness. Fig. (5) illustrates the XRD patterns of $ZnTe$ thin films of different thicknesses on glass substrates after $O^- - PIII$. This figure shows that the intensity peaks are broader than the same peaks before $O^- - PIII$. The broadened in XRD thin film peaks are due to instrumental and microstructure parameters (crystallite size and lattice strains) [11]. The pure line profile is extracted by deconvoluting the instrumental broadening factor from the experimental line profile. The pure line profile can be used for calculating the microstructure parameters, crystallite size and microstrain. In this work, the instrumental broadening-corrected of pure breadth of each reflection was calculated from the parabolic approximation correction [11]:

$$\beta(2\theta) = \sqrt{\beta_{obs}^2 - \beta_{ref}^2} (rad) \qquad (1)$$
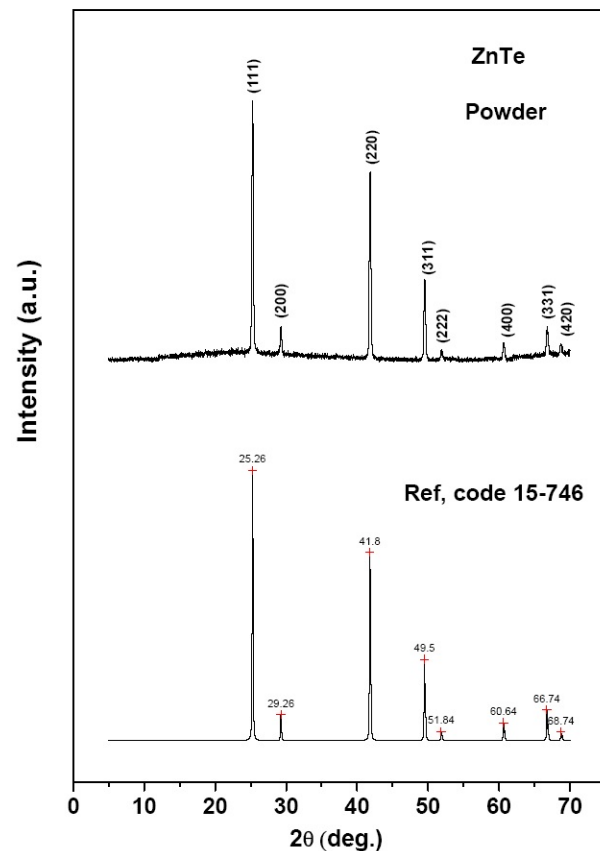

Fig. 3: X-ray diffraction spectra of ZnTe powder. The lower curve in figure represent a simulate scan from pattern according to ZnTe cards using X'Pert HighSore (version 1.0e) program.

where β_{obs} and β_{ref} are the breadth (in radians) of the same Bragg-peak from the XRD scans of the experimental and reference powder, respectively. The reference powder was of $ZnTe$ annealed at $300C$ for $2h$. Table (1) shows the values of $\beta(2\theta)$ for each reflection at different thickness of $ZnTe$ thin films. The breadth decreases at each reflection with increasing the film thickness for $ZnTe$ thin films. The method that based on the separation of crystallite size and strain takes the following form [12]:

$$\beta(2\theta)cos(\theta_0) = \frac{\lambda}{D_v} + 4esin(\theta_0) \qquad (2)$$

Fig. 6(a,b) illustrates the plot of $\beta(2\theta_0)cos(\theta_0)$ vs $sin(\theta_0)$ for $ZnTe$ thin films before and after $O^- - PIII$ for calculating the value of the crystallite size, (D_v) and lattice strain,) (e) from the slope and the ordinate intersection respectively. Eq. (2) was first used by Williamson and Hall [12] and is customarily referred to as the "Williamson-Hall method" [13,14,15]. Table (1) shows a (D_v) and (e) of different thickness of ZnTe thin
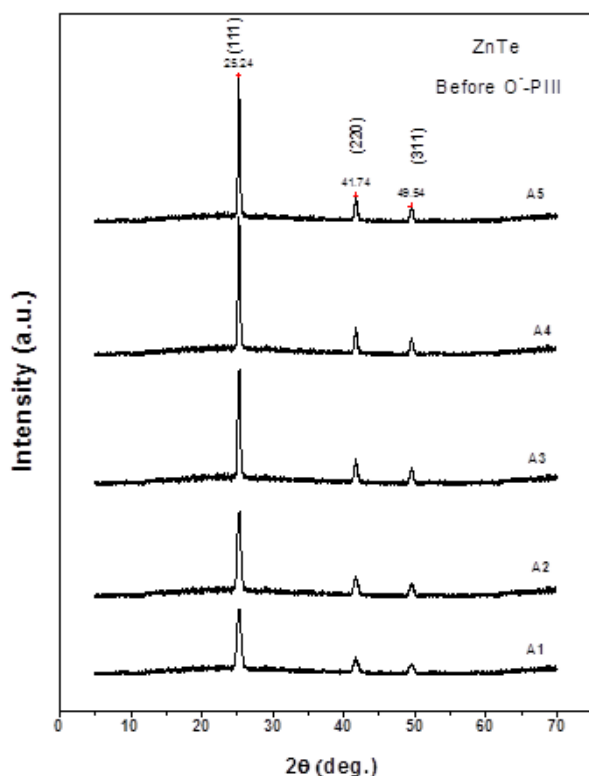
Fig. 4: The XRD patterns of ZnTe films of different thickness on glass substrates before $O^- - PIII$.

Fig. 5: : The XRD patterns of ZnTe films of different thickness on glass substrates after O^--PIII.

Table 1: Comparative look of the breadth, crystallite size and microstrain of *ZnTe* nanoparticle thin films with different thicknesses.

Samples	$\beta(2\theta)$			Crystallite	Micro-Strain
			D_v (nm)	size $eX10^{-3}$	
ZnTe	(111)	(220)	(311)		
Powder	0.2561	0.2691	0.0.2681		
A1	0.6687	0.0.7704	0.8212	18.041	2.255
A2	0.5515	0.6438	0.6768	23.323	1.982
A3	0.491	0.5599	0.6055	27.953	1.812
A4	0.456	0.524	0.5555	30.833	1.628
A5	0.4391	0.511	0.5321	32.633	1.581

Table 2: Comparative look of the breadth, crystallite size and microstrain of *ZnTe* nanoparticle thin films with different thicknesses after $O^- - PIII$.

Samples	$\beta(2\theta)$			Crystallite	Micro-Strain
			D_v (nm)	$size eX10^{-3}$	
ZnTe	(111)	(220)	(311)		
Powder	0.2561	0.2691	0.0.2681		
A1	0.7171	0.8261	0.8806	16.549	2.39
A2	0.5914	0.6904	0.7258	21.172	2.087
A3	0.5265	0.6004	0.6493	25.105	1.897
A4	0.489	0.5619	0.5957	27.47	1.695
A5	0.4708	0.5479	0.5706	28.947	1.641

films. It is observed that the (D_v) increases with increase the film thickness, but (e) exhibited an opposite behavior. This behavior may be attributed to the decrease in lattice defects among the grain boundary, where the grain size increases.

Table (2) also shows that the breadth increases after $O^- - PIII$ thus the crystallite size decrease according to "Williamson-Hall method". But the value of microstrain after $O^- - PIII$ increases in comparable with microstrain before $O^- - PIII$. Table2 shows the values of (D_v) and (e) $O^- - PIII$. The decrease in crystallites size and increase in microstrain may be attributed to the increase the stresses after $O^- - PIII$.
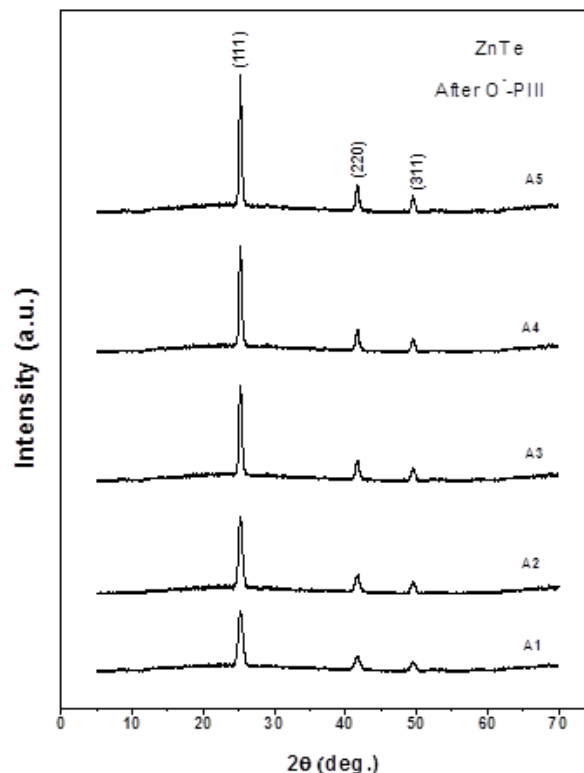
3.2 Optical properties of ZnTe before and after $O^- - PIII$.

Fig. (7) extended from $A1$ to $A5$ show that the transmittance of the five different thicknesses of as deposited and treated in oxygen of *ZnTe* thin films. This figures show that the transmittance is drastically improved by $O^- - PIII$ and the extremes of interference shifted towards the lower wavelengths. Swanepoel's method [16] has been employed extensively by many researchers [8,16,17,18,19], to calculate the refractive index and thickness of the thin films. Swanepoel's method based on a creation of top and bottom envelopes to the
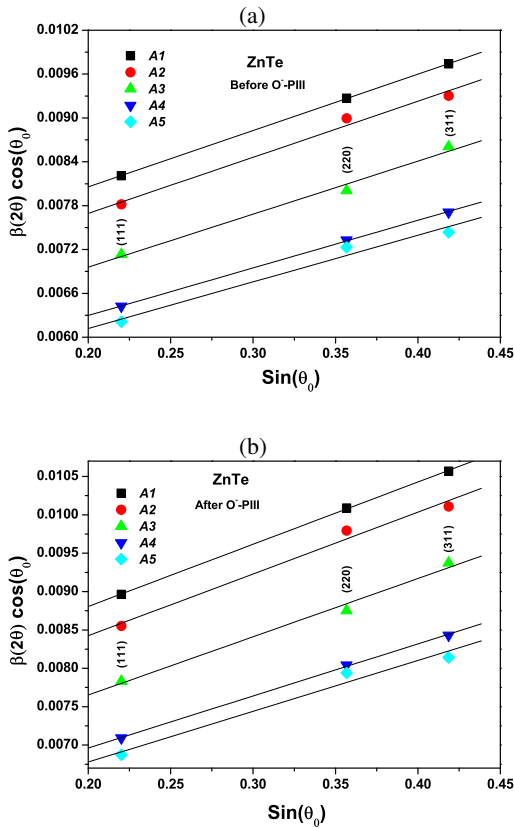
Fig. 6: (a) Crystallite size and lattice strain separation calculating using $\beta 2(\theta)cos\theta_0$ versus $sin(\theta_0)$ according to Williamson Hall method (a) before O$^-$-PIII. (b) The same as (a) but after O$^-$-PIII.
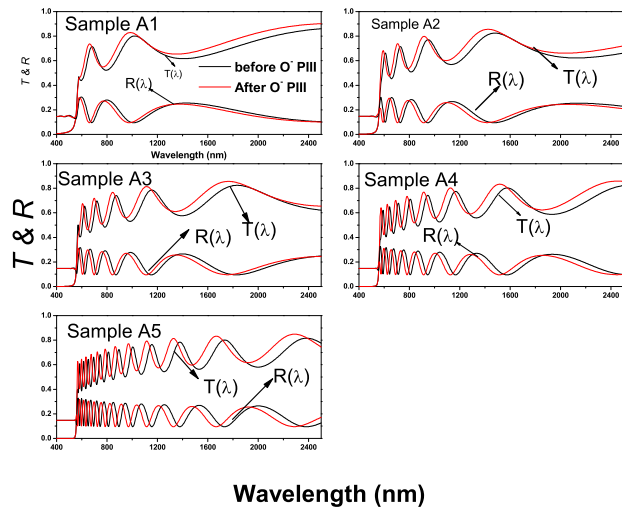

Fig. 7: five typical transmission and reflection spectrum for samples extended from A1 to A5 of different thickness of polycrystalline ZnTe thin films before and after O$^-$-PIII
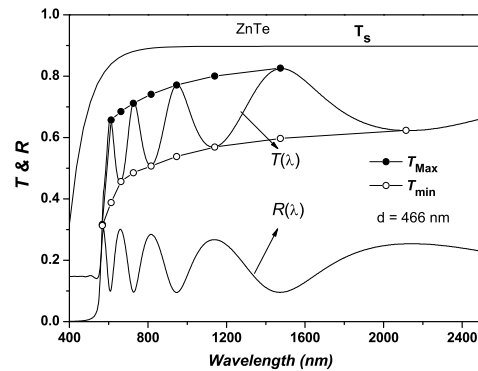
Fig. 8: The typical transmission spectra for sample A2 of *ZnTe* thin films. Curves T_{Max}, T_{min}, and $T\alpha$, according to the text.

interference maxima and minima observed in transmittance spectra as shown for example Fig. (8) . A first approximate value of the refractive index of the film n_1, in the spectral region of medium and weak absorption, can be calculated by the expression

$$n = [N + (N^2 - S^2)^{1/2}]^{1/2} \qquad (3)$$

where $N = 2S\frac{T_M - T_m}{T_M T_m} + \frac{S^2 + 1}{2}$ where T_M and T_m are the transmission maximum and the corresponding minimum at a each wavelength.

Alternatively, one of these values is an experimental interference extreme and the other one is derived from the corresponding envelope; both envelopes were computer-generated using the origin version 7 program using more than one procedure. On the other hand, the necessary values of the refractive index of the substrate are obtained from the transmission spectrum of the substrate, T_s using the well-known equation [20]:

$$S = \frac{1}{T_s} + (\frac{1}{T_s} - 1)^{1/2} \qquad (4)$$

The values of the refractive index n, as calculated from Eq. (2) are shown in Table (3). The accuracy of this initial estimation of the refractive index is improved after calculating d, as will be explained below. Now, it is necessary to take into account the basic equation for interference fringes

$$2nd = m\lambda \qquad (5)$$

where the order numbers m is integer for maxima and half integer for minima. Moreover, if n_{el} and ne2 are the refractive indices at two adjacent maxima (or minima) at λ_1 and λ_2, it follows that the film thickness is given by the expression

$$d = \frac{\lambda_1 \lambda_3}{2(\lambda_1)n_{e3} - \lambda_3)n_{e1}} \qquad (6)$$

Table 3: Values of λ, T_M and T_m of various thickness of *ZnTe* thin films corresponding to transmission spectra of Figure (1); the values of transmittance are calculated by orgin program. The calculated values of refractive index and film thickness are based on the envelope method before $O^- - PIII$.

Sample	λ	T_M	T_m	s	n_1	$d_1(nm)$	m_0	m	$d_2(nm)$	n_2
A1	674	0.71	0.488	1.533	2.632	0	2.55	2.5	320.1	2.723
	798	0.765	0.521	1.538	2.601	343.9	2.128	2	306.8	2.579
	1010	0.802	0.569	1.54	2.475	309.1	1.6	1.5	306	2.448
	1426	0.832	0.617	1.531	2.341	0	1.072	1	304.6	2.305
			d_2= 309.4nm	$\sigma_2 = 7.2nm(2.3\%)$						
A2	726	0.712	0.485	1.535	2.655	0	3.584	3.5	478.6	2.724
	816	0.741	0.507	1.538	2.617	516.5	3.143	3	467.7	2.624
	946	0.771	0.538	1.54	2.544	480.9	2.635	2.5	464.9	2.535
	1140	0.801	0.569	1.539	2.471	472.7	2.124	2	461.4	2.444
	1474	0.826	0.597	1.53	2.404	0	1.599	1.5	459.8	2.37
			d_1=490.04 nm	$\sigma_1 = 23.28nm(4.7\%)$		d_2=466.48nm	$\sigma_2 = 7.4nm(1.5\%)$			
A3	666	0.676	0.443	1.533	2.796	0	5.076	5	595.4	2.855
	718	0.692	0.462	1.535	2.731	644.2	4.598	4.5	591.6	2.77
	784	0.716	0.482	1.537	2.683	633.8	4.138	4	584.4	2.689
	870	0.741	0.506	1.539	2.623	599.5	3.644	3.5	580.5	2.611
	986	0.761	0.531	1.54	2.552	585.5	3.129	3	579.5	2.536
	1154	0.782	0.554	1.538	2.493	587.1	2.612	2.5	578.6	2.473
	1404	0.804	0.577	1.532	2.438	576.8	2.1	2	575.8	2.407
	1828	0.824	0.604	1.521	2.365	0	1.564	1.5	579.8	2.351
			d_1=604.48nm	$\sigma_1 = 27.89nm(4.7\%)$		d_2=583nm	$\sigma_2 = 6.85nm(1.1\%)$			
A4	712	0.677	0.446	1.535	2.784	0	6.587	6.5	831.3	2.844
	754	0.693	0.46	1.536	2.748	899.8	6.141	6	823.1	2.78
	806	0.71	0.476	1.538	2.703	854.2	5.651	5.5	819.9	2.724
	868	0.726	0.493	1.539	2.656	850.9	5.155	5	817.1	2.667
	944	0.742	0.509	1.54	2.611	839.3	4.661	4.5	813.4	2.611
	1042	0.758	0.526	1.54	2.567	833.1	4.151	4	811.8	2.561
	1166	0.773	0.542	1.538	2.526	831.7	3.649	3.5	807.9	2.508
	1334	0.788	0.559	1.534	2.485	818.8	3.138	3	805.3	2.459
	1570	0.802	0.574	1.527	2.442	811.2	2.621	2.5	803.6	2.412
	1930	0.813	0.587	1.52	2.405	0	2.1	2	802.4	2.372
			d_1=842.37 nm	$\sigma_1 = 27.37nm(3.2\%)$		d_2= 813.58 nm	$\sigma_2 = 9.43nm(1.14\%)$			
A5	746	0.677	0.451	1.536	2.755	0	9.567	9.5	1286	2.818
	776	0.688	0.46	1.537	2.733	1383	9.123	9	1278	2.777
	812	0.7	0.471	1.538	2.705	1353	8.63	8.5	1276	2.745
	850	0.711	0.481	1.539	2.679	1277	8.166	8	1269	2.704
	892	0.722	0.49	1.54	2.658	1346	7.718	7.5	1259	2.66
	946	0.733	0.501	1.54	2.631	1304	7.203	7	1259	2.633
	1002	0.742	0.511	1.54	2.601	1289	6.724	6.5	1252	2.59
	1074	0.754	0.523	1.539	2.57	1281	6.198	6	1254	2.563
	1154	0.764	0.534	1.538	2.545	1285	5.713	5.5	1247	2.524
	1256	0.773	0.544	1.536	2.517	1239	5.19	5	1248	2.497
	1380	0.781	0.554	1.533	2.487	1257	4.668	4.5	1249	2.469
	1532	0.79	0.564	1.528	2.46	1263	4.16	4	1245	2.437
	1732	0.799	0.573	1.523	2.435	1266	3.642	3.5	1245	2.411
	1998	0.808	0.581	1.52	2.42	0	3.137	3	1239	2.384
			d_1=1295.25 nm	$\sigma_1 = 43.57nm(3.36\%)$		d_2= 1257.57 nm	$\sigma_2 = 14.36nm(1.14\%)$			

The values of d of different samples determined by this equation, are listed as d_1, in Table (3). The average value of d_1, (ignoring the last two values). This value can now be used, along with n_1, to calculate the "order number" m_0 for the different extremes using Eq. (4).The accuracy of d can now be significantly increased by taking the corresponding exact integer or half integer values of m associated to each extreme Fig. (8) and deriving a new thickness, d_2 from Eq. (5), again using the values of n_1, the values of d found in this way have a smaller dispersion ($\sigma_1 > \sigma_2$). It should be emphasized that the accuracy of the final thickness is better than 1% Table (3). With the exact value of m and

the very accurate value of Eq. (5) can then be solved for n at each λ and, thus, the final values of the refractive index n_2 are obtained Table (3). Table (3 & 4) show the values of λ, T_M, T_m and the calculated values of refractive index and film thickness, which based on the envelope method for the investigated samples before and after $O^- - PIII$ of polycrystalline *ZnTe*.

Fig. (9) extended from *A*1 to *A*5 illustrate the dependence of n on wavelength for different thickness of *ZnTe* before and after O^-PIII. This figure illustrates that the change in the film thickness of polycrystalline *ZnTe* causes an increasing in the refractive index till 814*nm*

Table 4: Values of λ, T_M and T_m of various thickness of *ZnTe* thin films after O^--PIII corresponding to transmission spectra of Figure (1); the values of transmittance are calculated by orgin program. The calculated values of refractive index and film thickness are based on the envelope method after O^--PIII.

Sample	λ	T_M	T_m	s	n_1	d_1(nm)	m_0	m	d_2(nm)	n_2
A1	656	0.736	0.517	1.532	2.551	321.4	2.554	2.5	321.4	2.659
	774	0.793	0.549	1.537	2.538	305	2.153	2	305	2.51
	980	0.831	0.603	1.54	2.402	305.9	1.61	1.5	305.9	2.383
	1368	0.864	0.655	1.533	2.27	301.3	1.09	1	301.3	2.218
			d_2= 308.4nm	$\sigma_2 = 8.9nm(2.9\%)$						
A2	704	0.734	0.506	1.534	2.603	0	3.621	3.5	473.3	2.659
	794	0.764	0.534	1.538	2.542	505.1	3.135	3	468.6	2.571
	912	0.793	0.566	1.54	2.469	492.4	2.652	2.5	461.7	2.461
	1098	0.826	0.601	1.539	2.4	471.4	2.14	2	457.5	2.37
	1420	0.858	0.632	1.531	2.339	0	1.613	1.5	455.4	2.299
			d_1=489.6 nm	$\sigma_1 = 17nm(3.5\%)$		d_2=463.3nm	σ_2=7.5nm(1.6%)			
A3	648	0.698	0.463	1.532	2.734	0	5.106	5	592.4	2.799
	698	0.714	0.484	1.534	2.664	627.4	4.618	4.5	589.5	2.714
	760	0.738	0.509	1.537	2.601	628.9	4.142	4	584.3	2.626
	842	0.764	0.534	1.539	2.544	615.8	3.656	3.5	579.2	2.546
	952	0.788	0.56	1.54	2.486	602.6	3.159	3	574.5	2.467
	1108	0.812	0.586	1.539	2.429	587	2.652	2.5	570.3	2.393
	1348	0.836	0.612	1.534	2.371	568.5	2.129	2	568.5	2.329
	1764	0.856	0.635	1.522	2.315	0	1.588	1.5	571.5	2.286
			d_1=605.04nm	$\sigma_1 = 23.78nm(3.95\%)$		d_2=578.8 nm	$\sigma_2 = 9.1nm(1.6\%)$			
A4	692	0.7	0.469	1.534	2.709	0	6.633	6.5	830.1	2.781
	732	0.716	0.485	1.536	2.667	884.1	6.172	6	823.5	2.715
	782	0.732	0.502	1.537	2.619	866.4	5.675	5.5	821	2.659
	840	0.749	0.52	1.539	2.575	882.2	5.194	5	815.4	2.596
	912	0.765	0.536	1.54	2.538	873.5	4.714	4.5	808.5	2.537
	1004	0.783	0.553	1.54	2.504	843.2	4.224	4	802	2.483
	1124	0.802	0.572	1.539	2.461	812.3	3.71	3.5	799.1	2.432
	1286	0.819	0.592	1.535	2.415	804.5	3.182	3	798.7	2.385
	1512	0.834	0.61	1.529	2.371	810.1	2.657	2.5	797	2.337
	1854	0.848	0.624	1.52	2.338	0	2.136	2	793.1	2.292
			d_1=847.04 nm	$\sigma_1 = 33.97nm(4.01\%)$		d_2= 808.8 nm	$\sigma_2 = 12.9nm(1.6\%)$			
A5	722	0.7	0.472	1.535	2.695	0	9.555	9.5	1273	2.75
	752	0.714	0.482	1.536	2.676	1396	9.11	9	1265	2.714
	786	0.727	0.493	1.537	2.652	1312	8.638	8.5	1260	2.679
	824	0.736	0.505	1.538	2.618	1149	8.134	8	1259	2.643
	866	0.745	0.516	1.539	2.583	1301	7.635	7.5	1257	2.604
	914	0.756	0.528	1.54	2.553	1326	7.15	7	1253	2.566
	970	0.768	0.54	1.54	2.527	1328	6.67	6.5	1247	2.528
	1036	0.781	0.552	1.54	2.504	1303	6.186	6	1241	2.493
	1116	0.794	0.564	1.539	2.479	1276	5.687	5.5	1238	2.461
	1210	0.803	0.575	1.537	2.45	1260	5.183	5	1235	2.426
	1326	0.812	0.587	1.534	2.42	1249	4.671	4.5	1233	2.393
	1474	0.823	0.598	1.53	2.395	1232	4.159	4	1231	2.364
	1670	0.833	0.608	1.524	2.37	1229	3.632	3.5	1233	2.344
	1928	0.84	0.617	1.52	2.347	0	3.117	3	1232	2.319
			d_1=1280.08 nm	$\sigma_1 = 62.8nm(4.9\%)$		d_2= 1246 nm	$\sigma_2 = 14.1nm(1.13\%)$			

after that one can expect the increasing of *n* lies within experimental error.

The calculated value of *n* and *d* for treated samples by $O^- - PIII$, the value of interference order *m* is still the same in comparable with untreated samples i.e, the film thickness is still the same. The improvement of refractive transmittance leads to a decrease in refractive index in comparable with the refractive index before $O^- - PIII$ as illustrated in Fig. (9) extended from *A*1 to *A*5. Now, the values of n_2 as shown in table 3 and 4 can be fitted to a reasonable function such as the two-term Cauchy dispersion relationship, $n(\lambda) = a + b/\lambda^2$, which can be

used for extrapolation the whole wavelengths [21, 22] (see Fig. (3)).

The least squares fit of the two sets of values of n_2 for the different thickness samples before and after $O^- - PIII$ are listed in Table (5). The absorption coefficient, can be obtained in the strong absorption region in terms of experimentally measured values of T and R using the known equation [23]:

$$\alpha = \frac{1}{d}ln[\frac{(1-R)^2 + [(1-R)^4 + 4T^2R^2]^{1/2}}{2T}]   (7)$$

where d is the sample thickness.

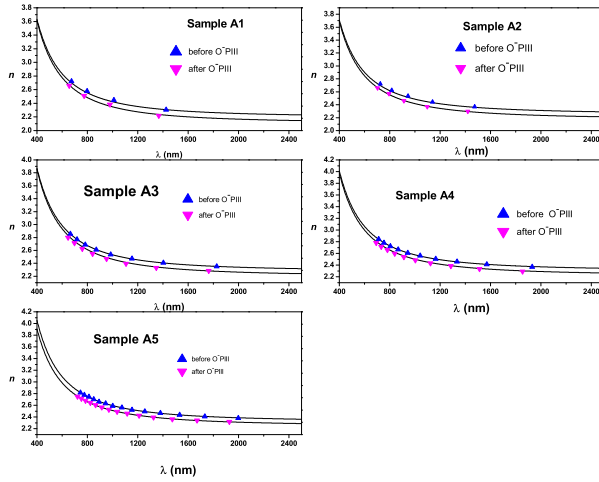**Fig. 9:** Refractive index dispersion spectra for *ZnTe* films before and after O$^-$-PIII.
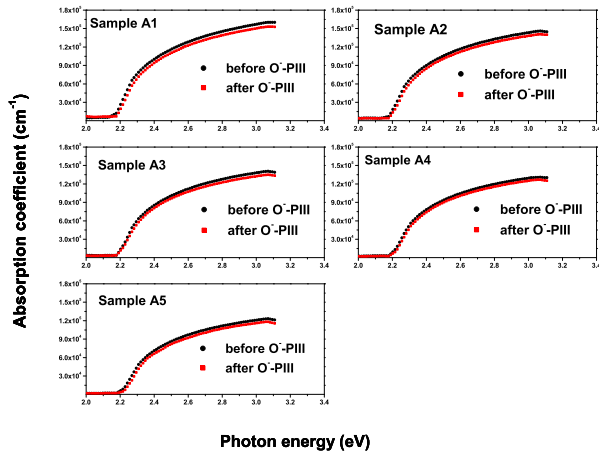

Fig. 10: The absorption coefficient against photon of *ZnTe* film samples before and after $O^- - PIII$.

Fig. (10) extended from A1 to A5 illustrate the absorption coefficient, versus photon energy for the different thickness samlpes before and after O–PIII. It is important to known that pure semiconducting compounds have a sharp absorption edge [18,24,25]. The absorption spectra for ZnTe thin films show that the respective films have a stoichiometric composition. For completing the calculation of the optical constants, the extinction coefficient, k is extracted from the values of α and λ using the known formula $k = \lambda \alpha / 4\pi$.

Fig. (11) extended from A1 to A5 show the dependence of k versus wavelength for different thickness samlpes before and after O–PIII. The vicinity of the fundamental absorption edge, for allowed direct band-to-band transitions, neglecting exciton effects, the

Table 5: Cauchy coefficient, optical band gap E_g^{opt} for different thickness of ZnTe thin films before and after $O^- - PIII$.

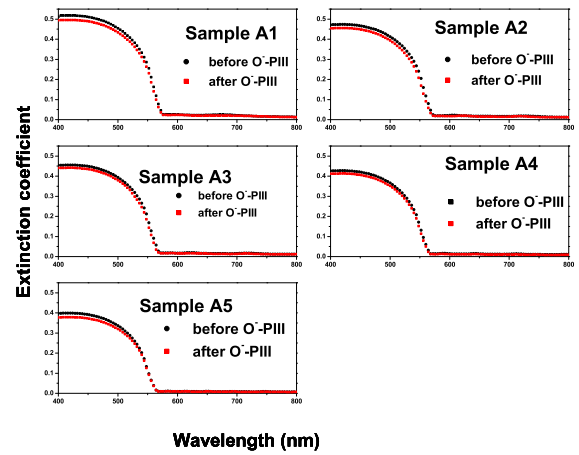| Samples		Cauchy coefficient		$E_g^{opt}(eV)$
		a	$b \times 10^5$	
	A_1	2.193	2.302	2.163
	A_2	2.253	2.341	2.184
Before O^- PIII	A_3	2.276	2.553	2.195
	A_4	2.303	2.74	2.211
	A_5	2.318	2.771	2.221
	A_1	2.107	2.405	2.185
	A_2	2.17	2.403	2.203
After O^- PIII	A_3	2.191	2.561	2.224
	A_4	2.222	2.571	2.231
	A_5	2.246	2.653	2.244

Fig. 11: The extinction coefficient versus wavelength of *ZnTe* film samples before and after $O^- - PIII$.

absorption coefficient is described by the

$$\alpha(h\nu) = \frac{k(h\nu - E_g^{opt})^p}{h\nu} \qquad (8)$$

where K is a characteristic parameter for respective transitions [26], $h\nu$ denotes photon energy, E_g^{opt} is optical energy gap and p is a number which characterizes the transition process. Different authors [17,19,27] have suggested different values of p for different glasses, $p = 2$ for amorphous semiconductors (indirect transition) and $p = 1/2$ for crystalline semiconductor (direct transition). In the case of different thickness of polycrystalline of *ZnTe* thin films the direct transition is valid.

Fig. (12) extended from $A1$ to $A5$ is a typical best fit of $(\alpha h\nu)^2$ versus photon energy $(h\nu)$ for different thickness of *ZnTe* thin films before and after $O^- - PIII$. The values of the direct optical band gap E_g^{opt} were taken as the intercept of $(h\nu)^2$ vs. $(h\nu)$ at $(\alpha h\nu)^2 = 0$ for the allowed direct transition. The estimated values of E_g^{opt} in this range of thicknesses of polycrystalline *ZnTe* films before and after $O^- - PIII$ listed in *Table*5.The optical band gap increase with increasing the film thickness. The

increase of E_g^{opt} for direct transition may be attributing to the increase in crystallites size. The increase of grain size with thickness can be attributed to the improved crystallinity. The improvement in crystallinity is due to increase ability of add atoms to move towards stable sites in the lattice. Thicker films are characterized by more homogeneous network, which minimizes the number of defects and localized states, and thus the optical band gap increases [28,29]. In all the spectra after $O^- - PIII$, sharp absorption is observed around the absorption edge and the fundamental absorption edge shifts towards the lower wavelength, i.e. the value of E_g^{opt} increases in comparable before $O^- - PIII$. This increase in energy gap may be attributed to the increase in closed packing of the atoms, thus the crystallinity increases after $O^- - PIII$
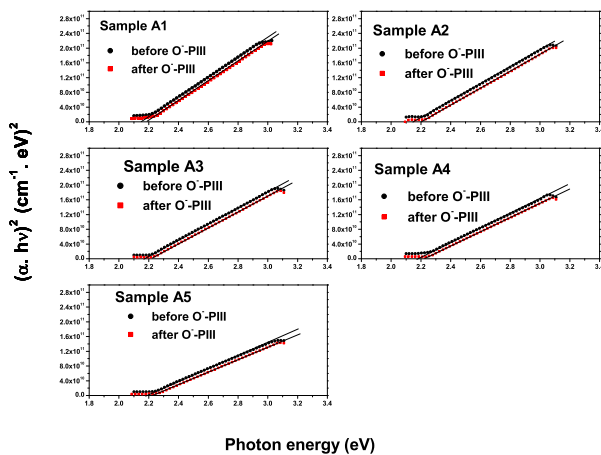

Fig. 12: The dependence of $(\alpha h\nu)^{1/2}$ on photon energy $h\nu$ for the five samples of polycrystalline $ZnTe$ thin films before and after $O^- - PIII$. From which the optical band gap E_g^{opt} is estimated.

4 Conclusions

Different thickness of Zinc telluride ($ZnTe$) thin films were deposited onto glass substrates in terms of the thermal evaporation technique. The experiments XRD of both powder and thin films of $ZnTe$ showed that the films are polycrystalline and have a zinc blende (cubic) structure. The calculated microstructure parameters of the $ZnTe$ thin films such as crystallite size (D_v) and microstrain showed that the size of crystallites increases with increasing the film thickness, while the microstrain shows an opposite variation trend due to the decrease in lattice defects, which were pronounced at small thicknesses. The effect of exposure to the oxygen plasma-immersion-ion-implantation ($O^- - PIII$) on the

structural and optical constants of the same samples of different thicknesses were also investigated. It is observed that the oxygen $PIII$ treatment can reduce both crystallize size and microstrain of $ZnTe$ thin films. Swanepoel's method has been applied in terms of transmittance spectra before and after $O^- - PIII$ to determine the refractive index and average thickness of the films. It is also observed that the oxygen $PIII$ treatment can effectively improve the transmission spectra of the samples particularly in medium and transparent regions, therefore the refractive index decrease. The optical constants and energy gap of different thickness of $ZnTe$ have been determined before and after oxygen plasma-immersion-ion-implantation ($O^- - PIII$). The increase of for direct transition may be also attributing to the increase in crystallites size and decrease in lattice strain. Thicker films are characterized by more homogeneous network, which minimizes the number of localized states. After $O^- - PIII$, the value of increases in comparable before $O^- - PIII$. This increase in energy gap may be attributed to the increase in closed packing of the atoms, thus the crystallinity increases after $O^- - PIII$.

Acknowledgement

References

[1] W. B. Jensen, *Journal of chemical education* **74**, 1063 (1997).

[2] M. P. Valkonen, S. Lindroos, M. Leskela and *Appl. Surf. Sci.* **134**, 283 (1998).

[3] I. T. Sinaoui, F. Chaffar Akkar, F. Aousgi and M. Kanzari, *Int. J. Thin Fil. Sci. Tec.* **3**, 19 (2014).

[4] K. C. Bhahada, B. Tripathi, N. K. Acharya, P. K. .Kulriya and Y. K. Vijay, *Appl. Surf. Sci.* **255**, 2143 (2008).

[5] G. I. Rusu, P. Prepelita, R. S. Rusu, N. Apetroaie, G. Oniciuc and A. Amariei, *J. Optoelectron. Adv. Mater.* **8** 922 (2006).

[6] Y. Ni, G. Yin, J. Hong and Z.Xu, *Mater. Res. Bull.* **39**, 1967 (2004).

[7] E. R. Shaaban,I.Kansal, S. H. Mohamed and J. M. F. Ferreira, *Physica B:* **404** , 3571 (2009).

[8] M. El-Hagary, M. Emam-Ismail, E. R. Shaaban and I. Shaltout, *J. Alloy Comp.* **485**, 519 (2009).

[9] E. R. Shaaban, E. A. A. Wahab and M. Ahmed, *Phys. Scr.* **88**, 015703 (2013).

[10] L. F. J. "*Ionization and Breakdown in Gases*", London; Methuen Co. (1956).

[11] X. Mathew, J. P. Enriquez, P. Sebastian, M. Pattabi, A. Sanchez-Juarez, J. Campos, J. C. McClure and V. P. Singh, *Sol. Energy Mater. Sol. Cells* **63**, 355 (2000).

[12] G. K. Williamson and H. W. H., *Acta Metallurgica* **1**, 22 (1953).

[13] D. G. Morris, M. A. Morris and M. LeBoeuf, *Materials Science and Engineering A* **156**, 11 (1992).

[14] G. H. Chen, C. Suryanarayana and F. H. Froes, *Metallurgical and Materials Transactions* **26A**, 1379 (1995).

[15] E. Szewczak, J. Paszula, A. V. Leonov and H. Matyja, *Materials Science and Engineering A* **A226**, 115 (1997).

[16] R. Swanepoel, *J. Phys. E: Sci. Instrum.* **17**, 896 (1984).

[17] E. M*a′*rquez, J.M. Gonza*′*lez-Leal, A.M. Bernal-Oliva, R. Jimnez-Garay and T. Wagner, *Journal of Non-Crystalline Solids* **354**, 503 (2008).

[18] E. R. Shaaban, *Mater. Chem. Phys.* **100**, 411 (2006).

[19] J. M. Gonzalez-Leal, R. Prieto-Alcon, J. A. Angel and E. Marquez, *J. Non-Cryst. Solids* **315**, 134 (2003).

[20] T. S. Moss, *Optical Properties of Semiconductors* (London: Buttenvorths) (1959).

[21] M. Emam-Ismail, E. R. Shaaban, M. El-Hagary and I. S. B. (2010), *Phil. Mag. B* **90**, 3499 (2010).

[22] E. R. Shaaban, M. A. Kaid, M. E. Sayed and A. Adel, *J. Phys. D Appl. Phys.* **41**, 125301 (2008).

[23] E. R. Shaaban, N. Afify and A. El-Taher, *J. Alloys & Comp.* **482**, 400 (2009).

[24] S. Chaudhuri, S. K.Biswas, and A. Choudhury, *J. Mater. Sci.* **23**, 4470 (1988).

[25] B. A. Mansour, H. Shaban, S. A. Gad, Y. A. EL-Gendy and A. M. Salem, *Journal of Ovonic Research*, **6**, 13 (2010).

[26] J. I. Pankove, *Optical Processes in Semiconductors* Dover, New York (1977), p. 44.

[27] E. A. Davis and N. F. Mott, *Philos. Mag.* **22**, 903 (1970).

[28] S. K.Biswas, S. Chaudhuri and A. Choudhury, *Phys. Status. Solidi (a)* **105**, 467 (1988).

[29] K.I. Arshak and C. Ahogarth, *Thin Solid Films* **137**, 281 (1986).